RAA 2019 Vol. **19** No. **1**, 7(12pp) doi: 10.1088/1674–4527/19/1/7

http://www.raa-journal.org *http://iopscience.iop.org/raa*

***R**esearch in*
***A**stronomy and*
***A**strophysics*

A multiwavelength view of a classical T Tauri star CV Cha

Jeewan Chandra Pandey, Subhajeet Karmakar, Arti Joshi, Saurabh Sharma, Shashi Bhushan Pandey and Anil Kumar Pandey

Aryabhatta Research Institute of Observational Sciences (ARIES), Nainital - 263002, India; *jeewan@aries.res.in*

Received 2018 April 19; accepted 2018 August 5

Abstract Using long-term optical, ultraviolet (UV) and X-ray data, we present a study of a classical T Tauri star CV Cha. The V-band light curve obtained from the All Sky Automated Survey (ASAS) shows short as well as long-term variability. The short-term variability could be due to rotational modulation of CV Cha. We derive the rotational period of 3.714 ± 0.001 d for CV Cha. UV light curves obtained from *Swift* also show the variations. X-ray light curves from *XMM-Newton* and *Swift* do not show any significant short as well as long-term variability. However, the light curve from *Chandra* appears to be variable, which could be due to the emergence of flaring activities. X-ray spectra from all observations are explained well by the single temperature plasma of 0.95 keV with X-ray luminosity of $10^{30.4}$ erg s^{-1} in the 0.5–7.5 keV energy band. It appears that variability in optical and UV bands could be due to the presence of both hot and cool spots on the surface, while X-ray emission is dominated by magnetic processes.

Key words: stars: activity — stars: individual (CV Cha) — stars: pre-main sequence — stars: variable: T Tauri — X-ray: stars

1 INTRODUCTION

Young (< 10 Myr) pre-main sequence (PMS) stars with a mass range of $0.5 - 2.5\,M_{\odot}$, spectral type of G to M and which are still accreting mass from their surroundings are known as T Tauri stars. The interior of a T Tauri star is either fully convective or possesses an outer convective envelope, depending on its age and mass. Stars with a circumstellar disc and equivalent width of the Hα line at 6563 Å of more than 10 Å are classified as classical T Tauri stars (CTTSs). It is believed that as a CTTS evolves toward the main sequence, the disc dissipates and the equivalent width of the Hα line becomes less than 10 Å, and the stars become what are known as weak-lined T Tauri stars (WTTSs). CTTSs have a magnetic field in the range of a few hundred to a few thousand Gauss (Johns-Krull 2007). This magnetic field truncates the inner disc near the corotation radius and channels circumstellar material from the disc onto the star (e.g. Shu et al. 1994; Bouvier et al. 2007). The circumstellar material falls down with nearly free-fall velocity onto the stellar surface, generating a shock and hot spots, which radiate in ultraviolet (UV) and soft X-ray wavebands (Kastner et al. 2002; Argiroffi et al. 2011). CTTSs show excess continuum emission in infrared (IR), optical and UV superimposed on the photospheric black-body spectrum. As mentioned above, the excess UV emission originates from the base of accretion shocks, whereas IR excesses are due to the absorption and re-emission of stellar photons by dust at the inner edges of the discs (Koenigl 1991). In addition to hot spots, cool spots are also thought to be present at the surface of a CTTS due to dynamo generated activity. Both hot and cool spots contribute to photometric variability of a CTTS (Bouvier et al. 1993b). We refer the reader to Hartmann et al. (2016) and Basri (2007) for recent reviews on T Tauri stars and their accretion process.

CV Cha is one of the brightest CTTSs in the Chamaeleon I dark cloud. This is a visual binary system with a rotation period of 4.25–4.4 d (Bouvier et al. 1986; Herbst & Koret 1988) that is located at a distance of 193 ± 1 pc (Lindegren et al. 2018). Its binary companion is CW Cha (spectral type M1D) with a binary separation of 11.4″ (Reipurth & Zinnecker 1993). CV Cha is classified as a spectral type of G8-K0 with a luminosity of $2.55\,L_{\odot}$, mass of $1.4\,M_{\odot}$ and radius of $2.5\,R_{\odot}$ (Rydgren 1980; Manara et al. 2016). This star has also been detected in X-

rays with the *Einstein Observatory* by Feigelson & Kriss (1989). Observations obtained with the *ROSAT* PSPC confirmed that CV Cha is one of the strongest X-ray sources in the Chamaeleon I dark cloud with an X-ray luminosity of $\sim 10^{30.12}$ erg s^{-1} (corrected for distance; Feigelson et al. 1993). Brooks et al. (2001) showed a very high level of activity in the atmosphere of CV Cha using *IUE* spectra. Using spectropolarimetric observations, Hussain et al. (2009) produced brightness and magnetic field maps of the surface of CV Cha and found the presence of dark polar caps and low-latitude spots. In this paper, we have analyzed the X-ray, UV and optical observations of CV Cha, which were taken from *Chandra, Swift, XMM-Newton* and the All Sky Automated Survey (ASAS).

This paper is organised as follows: Section 2 deals with observations and data reduction, Section 3 describes the timing analysis of observations made with ASAS, *Chandra*, *XMM-Newton* and *Swift*, X-ray spectral analysis is explained in Section 4, whereas kinematics and spectral energy distribution (SED) of CV Cha are given in Section 5, and finally in Section 6 we discuss our results and conclude.

2 OBSERVATIONS AND DATA REDUCTION

2.1 *Chandra*

The Chamaeleon I field was observed by the *Chandra* satellite using ACIS-I on 2001 July 08 @ 06:23:33 UT for ∼66.3 ks (P.I. - Feigelson, ID-1867). During the observation, two CCDs of ACIS-S were also active. The roll angle of the satellite was 242°. The ACIS-I observation of this field was analysed by Feigelson & Lawson (2004). Chandra version 4.8 along with the CALDB version 4.7.0 was used for the data reduction. We have also performed source detection in the ACIS-S2 CCD using the Palermo wavelet detection code, PWDetect[1] (Damiani et al. 1997). Source detection was applied after filtering the event in the 0.5–7.5 keV energy band. It analyses the data at different spatial scales, allowing the detection of both point-like and moderately extended sources, efficiently resolving close pairs. The detection threshold is an important input parameter in PWDETECT code, which can be estimated from the relationship between the background level and the expected number of spurious detections. The time-integrated background was estimated to be 0.04 counts arcsec^{-2} in the 0.5–7.5 keV energy band using the BACKGROUND task in XIMAGE. If we accept one spurious detection in the field of view then this background level translates into a detection threshold of 4.5. With this detection threshold, a total of five X-ray sources including CV Cha was detected in the ACIS-S2 CCD. One source, which was located at the edge of the CCD, was not detected. CV Cha was recorded in the S2 CCD of the ACIS-S array at 12.6′ away from the telescope centre. The source with RA = 11:12:31 and Dec = –79:42:34 was found to be the nearest X-ray source to the star CV Cha, which is 2.04′ away. There may be more X-ray sources in the field and nearby the star CV Cha, which could not be detected due to the poor point spread function (psf) at the off axes of *Chandra*. Therefore, further X-ray analyses can be taken with caution against possible contamination of nearby X-ray sources (if detected) to the selected source size in different detectors.

Light curve and spectra of the source were generated with the source region of elliptical size (semi-major axis = 15″, semi-minor axis = 10″), whereas the background was taken to be a source free region around the source. Selecting the size of the source region up to a few arcsec is safe as it does not include any other X-ray sources in its vicinity. Caution was also considered when selecting the size of background regions so that it should not contain any neighbouring source.

2.2 *XMM-Newton*

The *XMM-Newton* satellite observed the Chamaeleon I field using the European Photon Imaging Camera (EPIC) for ∼27.0 ks on 2004 September 28@18:47:46 UT in a revolution of 880 (P.I. - Telleschi, ID-0203810101). EPIC is composed of three CCDs behind three X-ray telescopes (Jansen et al. 2001); the twin metal oxide semiconductor (MOS) CCDs, MOS1 and MOS2 (Turner et al. 2001), and one p-n junction CCD, PN (Strüder et al. 2001). The data were reduced using the standard Science Analysis System (SAS) of *XMM-Newton*, version 16.0.0, with updated calibration files. CV Cha was detected ∼ 13.8′ away from the center of the PN detector, whereas in MOS detectors it was either detected at the edge or gap between the CCDs. Light curve and spectra were generated from on-source counts obtained from circular regions with a radius of 30″ around the source. The background was chosen from source-free regions on the same CCD in the detector surrounding the source. High background proton flares were recorded during the observation and were excluded from the data.

2.3 *Swift*

Swift observed CV Cha on 35 occasions (P.I.- Pandey, ID-000499930) from 2012 March 16 to 2016 February 29 us-

[1] *http://cerere.astropa.unipa.it/progetti_ricerca/PWDetect/*

ing its X-ray telescope (XRT; Burrows et al. 2005) and UV/optical telescope (UVOT; Gehrels et al. 2004). The exposure times for XRT observations were in the range of 113–3365 s, whereas exposure times for UVOT observations were in the range of 77–3345 s. The offsets of the XRT observations were in the range of $0.3' - 4.5'$. The XRT event files were filtered with the default screening criteria of xrtpipeline (V0.13.2). For every observation, the X-ray XSELECT (V2.4) package was used to extract images, light curves and spectra. For each observation, the X-ray light curves and spectra of CV Cha were extracted from on-source counts obtained from a circular region of $40''$ on the sky centred on the X-ray peaks, whereas, the background was extracted from source free circular regions. For the spectral analysis, ancillary response files were created using the task xrtmkarf and the latest response files (v015) were taken from the CALDB database.

The photometry for UVOT images was performed by using a region with radius of $5''$ to extract the source counts, whereas the background counts were extracted using an annular region with inner and outer radii of $20''$ and $30''$, respectively. The task UVOTMAGHIST was used to extract the background subtracted counts.

2.4 ASAS V-Band Observations

CV Cha was observed from 2000 December 3 to 2009 December 3 by ASAS[2] (Pojmanski 2002). We used grade "A" data within $5''$ of the target CV Cha. ASAS photometry provides five sets of magnitudes corresponding to five aperture values varying in size from 2 to 6 pixels in diameter. We found that magnitudes corresponding to the third aperture have minimal errors. Therefore, we took magnitudes corresponding to the third aperture for further analysis.

3 LIGHT CURVES AND VARIABILITY

3.1 V-Band

Figure 1(a) shows the V-band light curve of CV Cha as observed from ASAS. Both small and large scales of the variabilities are clearly seen. In order to derive the period from the data, we have performed periodogram analysis by using the method described by Scargle (1981). Power spectra computed with different methods are shown Fig. 1(b). A significant peak at a period of 2637 d is clearly seen in the Lomb-Scargle power spectrum. However, many other significant peaks are also present in the power spectrum and it is difficult to identify any other periodicity present in the data. Therefore, we have derived the window function of the data and over-plotted with the Lomb-Scargle power spectrum, to discard peaks which are due to the period gaps and other aliases. Many peaks corresponding to the long-term periods were not considered as they also show peaks in the window function (see left inset of Fig. 1(b)). Clusters of significant peaks around the frequency $\sim$0.27 were also observed and no window peak was seen at these frequencies. Further, to find the real peak in the clusters of peaks, we have used the CLEAN algorithm of Roberts et al. (1987). The cleaned power spectrum is also over-plotted in Figure 1(b). The CLEANed power spectrum presented here was obtained after 1000 iterations of the CLEAN procedure with a loop gain of 0.1. We found that the two frequencies corresponding to periods 2637 ± 59 d and 3.714 ± 0.001 d still persisted in the data (see the left and right insets of Fig. 1(b)). Further, these periods were above the 99% significance level. The significance level was determined by calculating the false alarm probability (Horne & Baliunas 1986). Presence of a short period of 3.714 could be due to the rotational modulation of CV Cha itself, whereas the long period could be due to presence of a long-term solar-type cycle.

Light curves of CV Cha were folded using the period 3.714 d and an epoch of HJD $= 2451869.85$, which is the first data point of ASAS observations. Folded light curves of CV Cha at different epochs are shown in Figure 2. The observational span is mentioned at the bottom of each panel in Figure 2. The observational spans were chosen in such a way that they can cover an entire phase with continuous observation. Phase coverage is fair to reasonably good in most of the light curves. However, for several time spans, we could not fold the light curve due to either the very sparse data or scattered data, or both. During the phase folding, we have also removed outliers from the light curves. It is also possible that these outliers may be due to the flaring episodes in CV Cha, but we could not confirm them as flaring events as there was only one data point above the regular variation of the star. To detect a flaring event, we need at least two consecutive data points above the regular variation, which was not possible with the present ASAS data due to very sparse observations (e.g., see Karmakar et al. 2016). Finally, folded light curves were binned to have 10–15 data points per rotational phase. At the top of each panel in Figure 2, amplitude, phase minimum and mean V-band magnitude are mentioned.

Figure 3 shows the variation of amplitude, phase of minimum and mean V-band magnitude of CV Cha with

[2] *http://www.astrouw.edu.pl/asas*

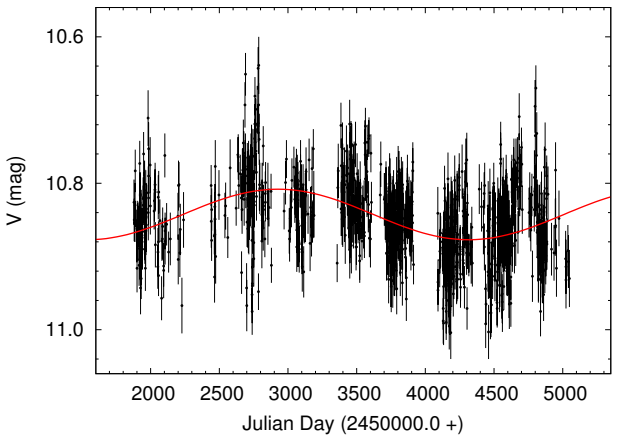

(a) V-band light curve

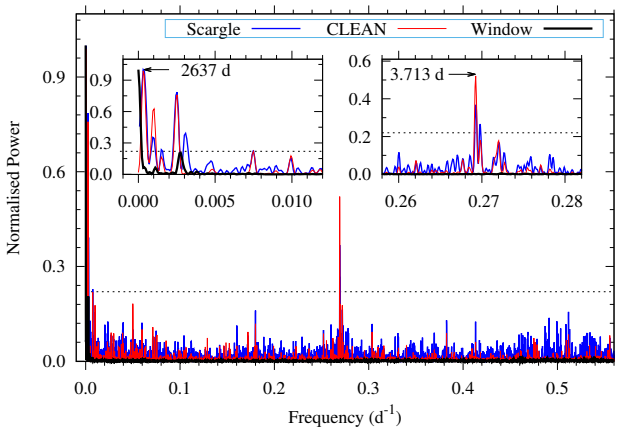

(b) Power spectra

Fig. 1 (a) V-band light curve of CV Cha as obtained from the ASAS data archive. The continuous curve is the best fit sine curve with a period of 2637 d. (b) Power spectra of V-band light curve as obtained using the Lomb-Scargle and CLEAN methods. The window function is also plotted. Zoomed views of power spectra near the periods of 2637 d and 3.71 d are shown in the left and right insets, respectively. Dashed horizontal lines represent the 99% significance level.

the central epoch of observations. The amplitude of these light curves was found to vary between 0.08–0.14 mag, whereas the phase of minima was also found to change its position from one epoch of observations to another. The phases of minima are clearly separated into two groups around the two straight lines as shown in Figure 3. The separation of these groups of phase minima is $\sim$180° in stellar longitude. In the initial epochs of observations, the phase minima were closer to each other, whereas in later epochs they were farther away. The mean value of stellar brightness was also varying from 10.82 mag to 10.9 mag, indicating long-term variations in the light curve.

3.2 UVOT

Figure 4(a) shows the UVOT light curve of CV Cha in U (3465 Å), W1 (2600 Å), W2 (2246 Å) and M2 (1928 Å) filters. The long-term variation was found to be present at all bands of UVOT. The UVOT light curves were folded using the ephemeris as derived above. Figure 4(b) shows the folded UVOT light curve of CV Cha in U (3465 Å), W1 (2600 Å), W2 (2246 Å) and M2 (1928 Å) filters. A rotational modulation was clearly seen in the U and W1 bands, whereas in M2 and W2 bands, the lack of phase coverage did not allow us to confirm the presence of rotational modulation. The mean values of the U, W1, M2 and W2 band magnitudes were 13.04 ± 0.02, 14.408 ± 0.005, 16.041 ± 0.007 and 16.001 ± 0.001 mag, respectively. The amplitude (maximum-minimum) in U and W1 bands was found to be 0.42 and 0.53 magnitude, respectively.

3.3 X-Rays

Figure 5 shows the background subtracted X-ray light curve in the 0.5–7.5 keV energy band as obtained from *Chandra*, *XMM-Newton* and *Swift*. The temporal binnings

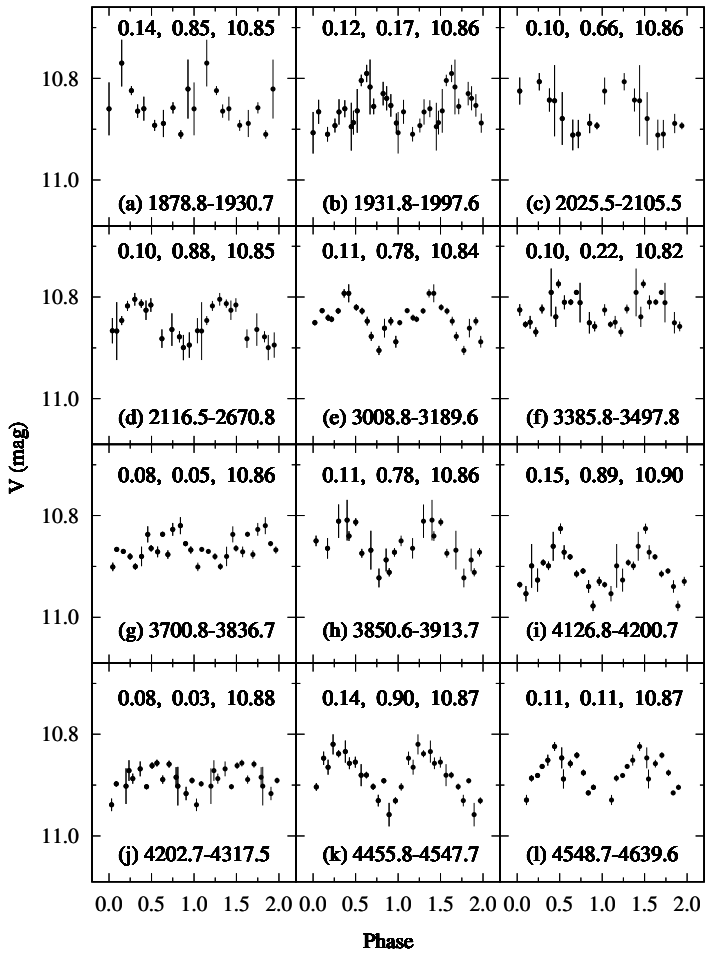

Fig. 2 V-band folded light curves of CV Cha at different epochs of ASAS observations. The observing duration is given at the bottom of each panel in JD (=2450000.0+). Parameters derived from the light curve are mentioned in the sequence amplitude, phase minimum and mean V-band magnitude at the top of each panel.

of *Chandra* and *XMM-Newton* light curves were 2000 and 500 s, respectively; whereas in the light curve from *Swift*, each observation was associated with each data point. The χ^2-test was performed in order to check the presence of variability in these light curves. The χ^2 was found to be 95.5(32), 47.4(42) and 19.5(23) for *Chandra*, *XMM-Newton* and *Swift* observations, respectively. Here the number in parentheses denotes the degrees of freedom. Comparing these values of the χ^2 statistic against a critical value of χ^2 for the 99.9% (χ^2_c) significance level, obtained from the χ^2-probability function, the light curve from *Chandra* was found to be variable with χ^2_c of 62, whereas two other light curves from *XMM-Newton* and *Swift* were found to be constant with χ^2_c of 66.2 and 49.7 respectively. From the *Chandra* light curve (see Fig. 5(a)), it is evident that the X-ray variability did not appear periodic. Initially, the *Chandra* light curve was constant up to 0.3 d of observations, then a slow rise followed by a slow decay was observed.

4 X-RAY SPECTRA

X-ray spectra of CV Cha as observed from three telescopes are shown in Figure 6. Observations from *Swift* were for a short exposure time, hence spectra obtained from these observations were very poor. During the observations no significant variability was found; therefore, in order to get meaningful spectra, we have added all the spectra using *addspec* from *Heasoft*. Further, all the spectra were rebinned to have at least 20 counts per spectral bin. Individual spectra from each observation were fitted with a thermal plasma model known as apec (Smith et al. 2001), with variable elemental abundances. The interstellar hydrogen column density ($N_{\rm H}$) was also left free to vary. A single temperature plasma model was found to be the best

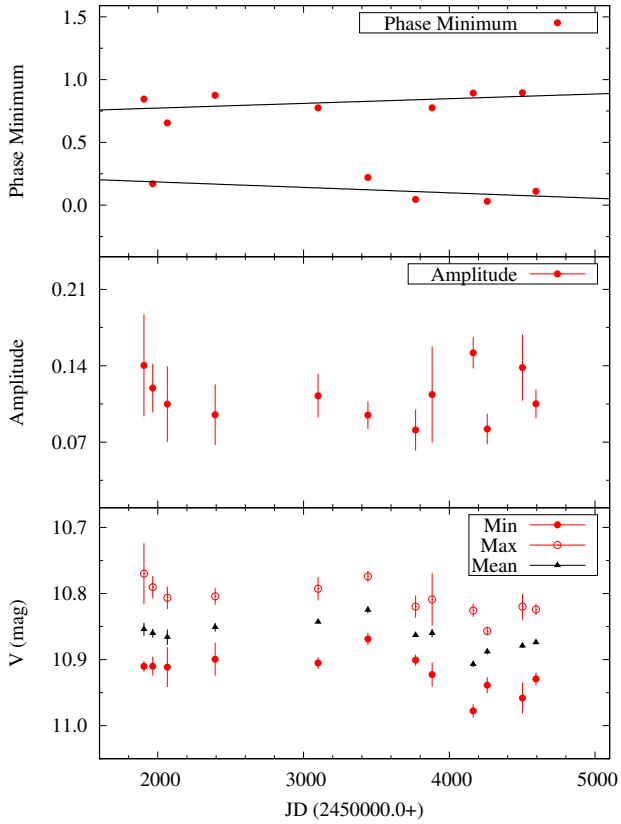

Fig. 3 Parameters obtained from V-band light curve. The average error in determination of phase minimum is 0.06.

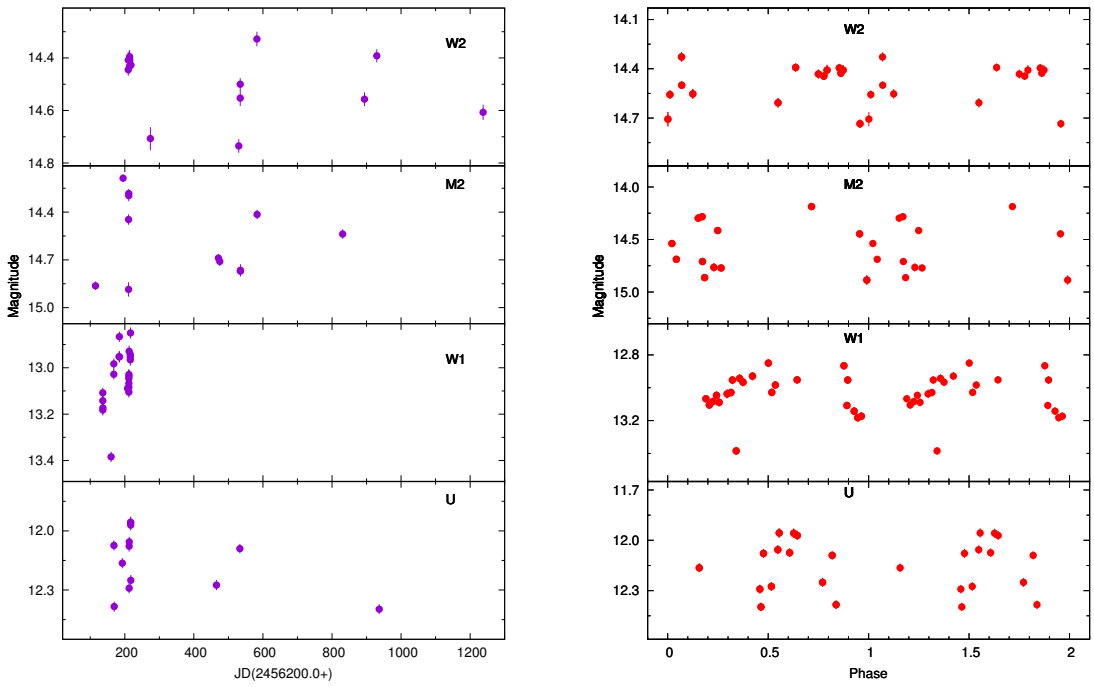

(a) UVOT light curve (b) Folded UVOT light curve

Fig. 4 (a) UVOT light curves of CV Cha as obtained from *Swift*. (b) Phase folded UVOT light curve of CV Cha. The central wavelengths of U, W1, M2 and W2 filters are 3465, 2600, 2246 and 1928 Å, respectively.

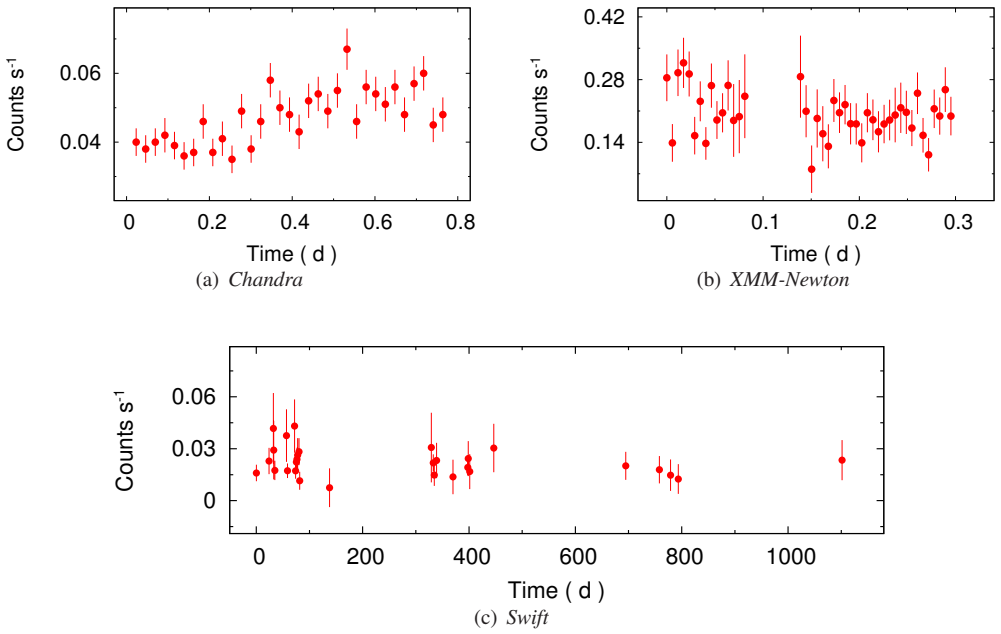

Fig. 5 X-ray light curves of CV Cha in the 0.5–7.5 keV energy band as observed from (a) *Chandra*, (b) *XMM-Newton* and (c) *Swift*.

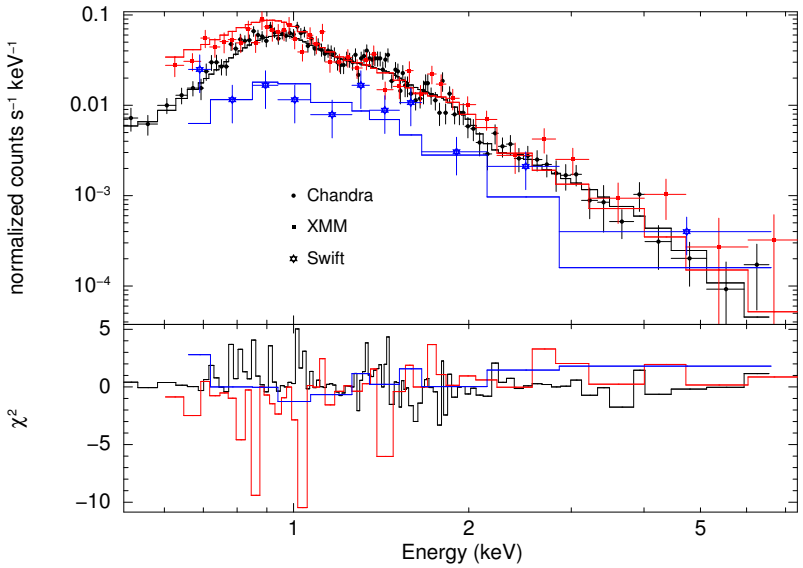

Fig. 6 X-ray spectra of CV Cha as observed from *Chandra*, *XMM-Newton* and *Swift* along with the best fit single temperature plasma model. Bottom panel shows the residual in terms of χ^2.

fit model for each spectrum. The best-fit parameters along with the reduced χ^2 are given in Table 1.

The error bars were estimated at the 90% confidence level from the minimum $\chi^2 + 2.71$. In order to obtain the average spectral parameters, the spectra from all observations were simultaneously fitted with a 1T model. The coronal temperature and corresponding emission measure were found to be 11.0 ± 0.4 MK and $2.3 \pm 0.3 \times 10^{53}$ cm^{-3}, respectively. The coronal abundances of CV Cha were found to be sub-solar at $0.08\,Z_{\odot}$, where $Z_{\odot}$ is solar photospheric abundance. The value of $N_{\rm H}$ was derived to be 1.9×10^{21} cm^{-2}. The unabsorbed X-ray luminosities in the 0.5–2.0 and 2.0–7.5 keV energy bands were derived to be $10^{30.18}$ and $10^{29.23}$ erg s^{-1}, respectively.

5 KINEMATICS AND SPECTRAL ENERGY DISTRIBUTION

Using the proper motion of $\mu_\alpha = -21.09 \pm 0.328$, $\mu_\delta = -0.859 \pm 0.291$ and parallax of $\pi = 5.03 \pm 0.22$ from *Gaia* (Lindegren et al. 2016) and radial veloc-

Table 1 The best fit spectral parameters. Distance of 199 ± 9 pc was taken from *Gaia* parallax.

Satellite ($\rightarrow$) Parameter ($\downarrow$)	*Chandra*	*XMM-Newton*	*Swift*	Average
kT (keV)	0.95 ± 0.05	0.97 ± 0.09	1.0 ± 0.2	0.97 ± 0.04
EM (10^{53} cm^{-3})	3.9 ± 0.3	4.7 ± 0.7	5.1 ± 2.0	4.2 ± 0.4
Z ($Z_{\odot}$)	0.10 ± 0.02	0.04 ± 0.02	0.04 ± 0.02	0.08 ± 0.01
$N_{\rm H}$ (10^{21} cm^{-2})	1.8 ± 0.3	2.2 ± 0.6	1.7 ± 0.7	1.9 ± 0.3
L (10^{30} erg s^{-1})				
(0.5–7.5 keV)	2.39 ± 0.03	2.33 ± 0.06	2.57 ± 0.11	2.38 ± 0.03
(0.5–2.0 keV)	2.10 ± 0.03	2.10 ± 0.06	2.17 ± 0.09	2.08 ± 0.02
(2.0–7.5 keV)	0.29 ± 0.01	0.33 ± 0.01	0.40 ± 0.02	0.30 ± 0.01
χ^2_{ν} (dof)	0.94(98)	1.23(38)	0.8(13)	1.07(156)

Notes: kT is plasma temperature; EM is emission measure; Z is abundance; $N_{\rm H}$ is hydrogen column density; L is X-ray luminosity; χ^2_{ν} is reduced χ^2 and dof is degrees of freedom.

ity of $15 \pm 0.2\,{\rm km\,s^{-1}}$ (de Bruijne & Eilers 2012), we have calculated the space velocity components (U, V, W) following Johnson & Soderblom (1987). The U, V and W components of space velocity were calculated to be -10.9 ± 0.4, -19.6 ± 0.7 and $-12.2 \pm 0.4\,{\rm km\,s^{-1}}$ respectively. Figure 7(a) shows the position of CV Cha in U-V-W space along with the 27 young moving groups (see Gagné et al. 2018). CV Cha is located close to the η Chamaeleontis association, whose age is $\sim$4 Myr.

The spectral energy distribution (SED) was also generated for CV Cha using the fluxes at wavelengths of 0.37, 0.55, 0.65, 0.80, 1.2, 1.6, 2.2, 3.6, 4.5, 5.8, 8.0, 12, 22, 24 and 70 μm. The optical data were taken from Henden et al. (2016), whereas the near-IR (NIR) and mid-IR (MIR) data were taken from 2MASS (Cutri et al. 2003), and *Spitzer*[3] and *WISE* (Wright et al. 2010) surveys, respectively. Figure 7(b) shows the SED of CV Cha. For characterizing and understanding the nature of CV Cha, the constructed SED was fitted using the model of Robitaille et al. (2006, 2007). The models were computed by using 20 000 2-D Monte-Carlo based radiation transfer calculations from Whitney et al. (2003a,b, 2004) and by adopting several combinations of a central star, a disc, an in-falling envelope and a bipolar cavity in a reasonably large parameter space and with 10 viewing angles (inclinations). The SED fitting tools provide the evolutionary stage and physical parameters such as mass, age, disc mass, disc accretion rate and stellar temperature of young stellar objects (YSOs) and hence are an ideal tool to study the evolutionary status of YSOs. The SED fitting tool fits each of the models to the data, allowing distance and extinction as free parameters. We further set photometric uncertainties of 10% for optical data and 20% for both NIR and MIR data. These values are adopted instead of the formal errors in the catalogue in order to fit without any possible bias caused by underestimating the flux uncertainties. We obtained the physical parameters of CV Cha using the relative probability distribution for the stages of all the 'well-fit' models. The well-fit models for each source are defined by $\chi^2 - \chi^2_{\rm min} \leq 2N_{\rm data}$, where $\chi^2_{\rm min}$ is the goodness-of-fit parameter for the best-fit model and $N_{\rm data}$ is the number of input data points. The best fit models along with the SED of CV Cha are shown in Figure 7(b), where the solid black curves represent the best-fit and the grey curves are the corresponding good-fits. As can be seen, the SED rises substantially in the MIR due to its optically thick disc. From the well-fitted models for each source derived from the SED fitting tool, we calculated the χ^2 weighted model parameters such as A_V, distance, stellar mass and stellar age of CV Cha and the best fit values of these parameters are given in Table 2. The error in each parameter is calculated from the standard deviation of all well-fit parameters. The derived values of age and mass are consistent to those derived by Manara et al. (2016).

Table 2 Parameters Derived from SED Fitting

A_V (mag)	1.1 ± 0.2
Mass ($M_{\odot}$)	1.3 ± 0.4
Radius ($R_{\odot}$)	3.0 ± 0.4
Age (Myr)	1.0 ± 0.5
Temperature (K)	4387 ± 309
Disc mass (gas + dust) ($M_{\odot}$)	$3.6 \pm 0.4 \times 10^{-2}$
Envelope accretion rate ($M_{\odot}$ yr^{-1})	$2.4 \pm 2.3 \times 10^{-8}$
Disc accretion rate ($M_{\odot}$ yr^{-1})	$7.1 \pm 2.1 \times 10^{-7}$

Hussain et al. (2009) estimated the various parameters of CV Cha using the PMS isochrones of Siess et al. (2000). They also used the extinction A_V of 1.67 and distance of 160 pc to determine the absolute magnitude and dereddened $(B-V)$ colour of CV Cha. From the ASAS obser-

[3] *http://ssc.spitzer.caltech.edu/*

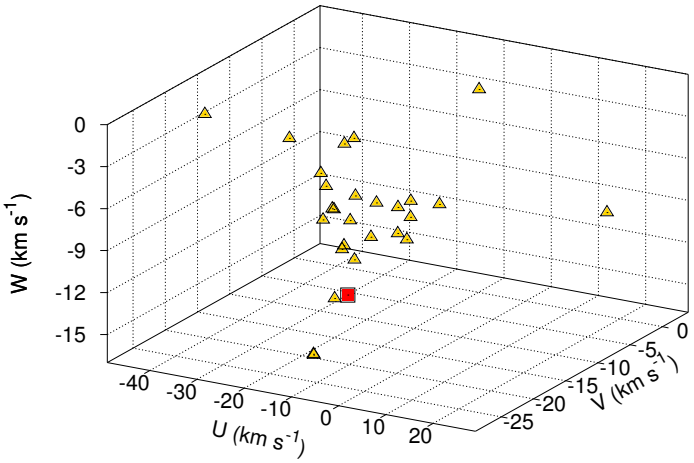

(a) U-V-W diagram

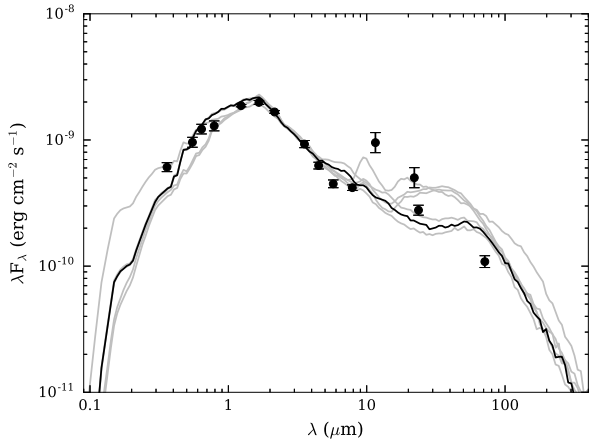

(b) SED

Fig. 7 (a) Plot between space velocity components (U, V and W) of CV Cha along with 27 young moving groups. CV Cha is represented by a *square* whereas young moving groups are represented by *triangles*. (b) SED of CV Cha along with the best model from Robitaille et al. (2006, 2007).

vation, the maximum brightness of CV Cha was also found to be varying between 10.77 and 10.85 mag. Using the average maximum-brightness in the V band of 10.8 mag, $A_V = 1.2$ mag (see Table 2 and Sect. 6), and much better known distance from *Gaia* parallax, we derive the absolute V-band magnitude of CV Cha as 3.1 mag. Using $E(B-V)$ of 0.38 (see Sect. 6) and $(B-V)$ colour of 1.07 mag (see Gauvin & Strom 1992; Henden et al. 2016), the dereddened $(B-V)$ was estimated to be 0.72 mag. Given these values, we have identified the evolutionary status of CV Cha using PMS isochrones of Siess et al. (2000). The age and mass of CV Cha were found to be $\sim$5.0 Myr and $\sim$1.6 $M_{\odot}$, respectively. The age produced from this method is slightly higher than that generated from the SED fitting method, whereas the derived value of mass is consistent with that yielded from the SED fitting method.

6 DISCUSSION AND CONCLUSIONS

Using the optical V-band light curve, we found the period of CV Cha to be 3.714 d, which is less than the previously derived period of 4.2–4.4 d (Bouvier et al. 1986; Bouvier & Bertout 1989; Herbst & Koret 1988). The previously derived period of CV Cha is somewhat uncertain. The presently derived period is from long-term data, therefore it can be considered as a reliable period. The folded light curves of CV Cha show variations in both the mean brightness and amplitude of rapid variability along the

variable shape of the light curve. Such variations are commonly seen in the optical light curves of cool active and T Tauri stars (e.g. Bouvier et al. 1993a; Pandey et al. 2005), which are interpreted as the presence of cool/hot spots on the surface of the CTTS. The amplitude of variation in the light curves of CV Cha is similar to that of the majority of CTTSs. The standard deviations of mean brightness and amplitude of 0.02 for each indicate stable variation over several years, which is common in a majority of CTTSs as studied by Grankin et al. (2007). As defined by Herbst et al. (1994), the variability in the optical light curves of PMS stars is expressed in three types: (i) rotation of cool spots on the stellar surface with a small amplitude (few 0.1 mag), (ii) rotation of an accretion related hot spot on the stellar surface with a large amplitude (up to 3 mag) and (iii) dips in luminosity due to obscuration of circumstellar dust which lasts from a few days to several months. Variability in the star CV Cha appears to be either Type I or Type II. Type I variations are mainly present in WTTSs but CTTSs also show this type of variability, whereas Type II variability is shown by a majority of CTTSs (Herbst et al. 1994; Grankin et al. 2007). The presence of two spots is clearly established by two well-separated straight lines in Figure 3. The separation in these two groups of spots is also found to be variable. The average separation between these two groups of spots is $\sim 180^{\circ}$. Such signatures are usually found in solar-type stars due to the presence of cool spots on their surface and interpreted as the different latitudinal position of spot groups. Apart from the short-term variability, a regular long-term variability was also noticed in its V-band light curve with an approximate period of $\sim$ 7 yr. Similar long-term variations were also found for many other CTTSs. This long-term periodic variation in CTTSs is generally explained due to the evolution of cool spots on the stellar surface. However, the long-term variations in CTTSs are also explained by the processes in the inner disc and in the accretion zone (e.g. Rigon et al. 2017). From the above discussion, it appears that both sources of variability (due to cold spots and hot spots) are likely to co-exist, similar to other CTTSs as described by Grankin et al. (2007).

In general, the chromosphere and transition region contribute significantly to the UV part of the electromagnetic spectrum of T Tauri stars. However, it is also accepted that CTTSs accrete mass from their discs via magnetospheric accretion, form shocks near the surface and emit energetic photons, which after re-processing in the accretion streams irradiate the inner disc with UV radiation (Ardila & Johns-Krull 2009). Present long-term UV observations from *Swift* show variability in all four bands. We did not see any regular pattern of variability in the M2 and W2 filters, whereas the variability in W1 and U filters appears to be rotationally modulated. The absence of any regular variability in the W2 and U2 filters could be due to a long observing span during which the activity level changed continuously. The amplitudes of variability in U and W bands are found to be more than that in the V-band. The amplitude of variability, in general, is found more in the UV band than in the optical band, if the variability is attributed to either accretion related or chromospheric features. In the current scenario, it is difficult to find the origin of UV variability. However, in the majority of CTTSs, the UV variability is related to accretion and a hot spot. Further, Ingleby et al. (2013) also showed that CV Cha has strong UV excesses above the stellar photospheric emission, which suggests a very strong mass accretion rate in CV Cha.

The X-ray emission from CV Cha is constant over the $\sim$3 years of *Swift* observations. No variability was seen in the X-ray light curve obtained from *XMM-Newton* for ~ 0.3 d. However, a small variability is found to be present in the *Chandra* ~ 0.8 d observations. A slow rise followed by slow decay was seen in the *Chandra* light curve, indicating that the variability could be due to the emergence of small-scale flares. From the X-ray spectral fittings, the average plasma temperature of CV Cha is derived to be 11.2 MK, which is in between that derived for other T Tauri stars (e.g. Getman et al. 2005). Furthermore, the plasma temperature was found to be constant over three different observations. We derived the X-ray luminosity of CV Cha as $10^{30.4}$ erg s^{-1} in the energy band of 0.5–7.5 keV. We did not find any significant variation in the X-ray luminosity from three observations. The X-ray luminosity in the soft energy band was $\sim$ 7 times higher than that of the hard energy band. This behaviour was found to be consistent among all three observations. This indicates that CV Cha is stronger in the soft energy band. The X-ray luminosity derived from these three observations is found to be more than that derived from earlier observations by *ROSAT* ($10^{30.15}$ erg s^{-1}; Feigelson & Kriss 1989) and the *Einstein Observatory* ($10^{30.1}$ erg s^{-1}; Feigelson et al. 1993). A more quantitative comparison of CV Cha with other CTTSs in the Chamaeleon I cloud indicates that it is one of the strongest X-ray emitters whose X-ray luminosity is similar to the most luminous CCTS WW Cha in the Chamaeleon I region (see Feigelson & Lawson 2004).

The X-ray emission in a CTTS is dominated by magnetic processes similar to solar activity (Feigelson &

Montmerle 1999). The X-ray emission is often variable with a flare-like structure, which is characterized by a rapid increase in the observed X-ray flux followed by a slow decay. During the flaring events in T Tauri stars, the plasma temperatures increase to extreme values of more than 100 MK (Getman et al. 2008). The other physical process that contributes to X-ray emission is the accretion process, which produces cool plasma with temperature less than 3 MK in the post-shock zone of an accretion shock at or near the surface (Kastner et al. 2002; Stelzer & Schmitt 2004; Brickhouse et al. 2010; Argiroffi et al. 2011). The shock temperature $= 3.44M/R$ (Calvet & Gullbring 1998) for CV Cha is calculated to be 1.5 MK, which is very low compared to that derived from X-ray spectral fitting. Here, M and R are mass and radius of the star respectively in terms of solar units. We have also computed the compactness of CV Cha as $M^{-1/2}R^{-3/2}$. Using the values of M and R as given in Table 2, the value of $M^{-1/2}R^{-3/2}$ is estimated to be 0.2. This value is in between those for various other CTTSs derived by Robrade & Schmitt (2007) and indicates a low electron density ($\sim 10^{10}$ cm^{-3}). In the cases of TW Hya and RU Lup, the value of $M^{-1/2}R^{-3/2}$ is more than 0.5, indicating high electron density and hence giving an indication of X-rays from the accretion phenomenon. Further, the majority of X-ray emission in T Tauri stars usually originates from hot magnetically confined coronae (Stassun et al. 2006). In this scenario, it appears that X-ray emission from CV Cha is also dominated by the magnetic process.

During the *Chandra* observation of CV Cha, the abundances were found to be slightly higher ($> 2\sigma$) than the other two observations. The derived average value of abundances of $0.1\ Z_{\odot}$ is similar to that of T Tauri stars, i.e. $0.1-0.3\ Z_{\odot}$ (e.g. Imanishi et al. 2001). From the X-ray spectral fitting, we find the value of $N_{\rm H}$ as $1.9 \pm 0.3 \times 10^{21}$ cm^{-2}, which corresponds to $E(B-V) = 0.38 \pm 0.07$ (see Vuong et al. 2003, for conversion formula). The derived value of $E(B-V)$ is similar to that derived from the SED fitting using the normal reddening law. This value of $E(B-V)$ is smaller than that derived by Brooks et al. (2001), but our derived value of $E(B-V)$ is similar to that reported in other earlier studies (Simon et al. 1985; Manara et al. 2016). The value of $N_{\rm H}$ was also found to be non-variable from three different observations.

In summary, we found that CV Cha is a periodic variable with a period of 3.714 d in which the observed modulation in optical and UV bands could be due to the mixture of both hot and cool surface spots, whereas the X-ray emission appears to be dominated by hot magnetically confined coronae.

Acknowledgements This work is based on data taken from the *Chandra*, *XMM-Newton* and *Swift* satellites. Pwdetect has been developed by scientists at Osservatorio Astronomico di Palermo. G. S. Vaiana thanks the Italian CNAA and MURST (COFIN) grants. JCP and SK acknowledge the DST-RFBR project INT/RUS/RFBR/P-271. SBP acknowledges BRICS grant number DST/IMRCD/BRICS/PilotCall1/ProFCheap/2017(G) for part of the present work. We acknowledge the referee of the paper for his/her useful comments.

References

Ardila, D. R., & Johns-Krull, C. M. 2009, in American Institute of Physics Conference Series, 1094, 15th Cambridge Workshop on Cool Stars, Stellar Systems, and the Sun, ed. E. Stempels, 309
Argiroffi, C., Flaccomio, E., Bouvier, J., et al. 2011, A&A, 530, A1
Basri, G. 2007, in IAU Symposium, 243, Star-Disk Interaction in Young Stars, eds. J. Bouvier, & I. Appenzeller, 13
Bouvier, J., Alencar, S. H. P., Harries, T. J., Johns-Krull, C. M., & Romanova, M. M. 2007, Protostars and Planets V, 479
Bouvier, J., & Bertout, C. 1989, A&A, 211, 99
Bouvier, J., Bertout, C., Benz, W., & Mayor, M. 1986, A&A, 165, 110
Bouvier, J., Cabrit, S., Fernandez, M., Martin, E. L., & Matthews, J. M. 1993a, A&AS, 101, 485
Bouvier, J., Cabrit, S., Fernandez, M., Martin, E. L., & Matthews, J. M. 1993b, A&A, 272, 176
Brickhouse, N. S., Cranmer, S. R., Dupree, A. K., Luna, G. J. M., & Wolk, S. 2010, ApJ, 710, 1835
Brooks, D. H., Costa, V. M., Lago, M. T. V. T., & Lanzafame, A. C. 2001, MNRAS, 327, 177
Burrows, D. N., Hill, J. E., Nousek, J. A., et al. 2005, Space Sci. Rev., 120, 165
Calvet, N., & Gullbring, E. 1998, ApJ, 509, 802
Cutri, R. M., Skrutskie, M. F., van Dyk, S., et al. 2003, VizieR Online Data Catalog, 2246
Damiani, F., Maggio, A., Micela, G., & Sciortino, S. 1997, ApJ, 483, 350
de Bruijne, J. H. J., & Eilers, A.-C. 2012, A&A, 546, A61
Feigelson, E. D., Casanova, S., Montmerle, T., & Guibert, J. 1993, ApJ, 416, 623
Feigelson, E. D., & Kriss, G. A. 1989, ApJ, 338, 262
Feigelson, E. D., & Lawson, W. A. 2004, ApJ, 614, 267
Feigelson, E. D., & Montmerle, T. 1999, ARA&A, 37, 363
Gagné, J., Mamajek, E. E., Malo, L., et al. 2018, ApJ, 856, 23
Gauvin, L. S., & Strom, K. M. 1992, ApJ, 385, 217

Gehrels, N., Chincarini, G., Giommi, P., et al. 2004, ApJ, 611, 1005
Getman, K. V., Feigelson, E. D., Grosso, N., et al. 2005, ApJS, 160, 353
Getman, K. V., Feigelson, E. D., Micela, G., et al. 2008, ApJ, 688, 437
Grankin, K. N., Melnikov, S. Y., Bouvier, J., Herbst, W., & Shevchenko, V. S. 2007, A&A, 461, 183
Hartmann, L., Herczeg, G., & Calvet, N. 2016, ARA&A, 54, 135
Henden, A. A., Templeton, M., Terrell, D., et al. 2016, VizieR Online Data Catalog, 2336
Herbst, W., Herbst, D. K., Grossman, E. J., & Weinstein, D. 1994, AJ, 108, 1906
Herbst, W., & Koret, D. L. 1988, AJ, 96, 1949
Horne, J. H., & Baliunas, S. L. 1986, ApJ, 302, 757
Hussain, G. A. J., Collier Cameron, A., Jardine, M. M., et al. 2009, MNRAS, 398, 189
Imanishi, K., Koyama, K., & Tsuboi, Y. 2001, ApJ, 557, 747
Ingleby, L., Calvet, N., Herczeg, G., et al. 2013, ApJ, 767, 112
Jansen, F., Lumb, D., Altieri, B., et al. 2001, A&A, 365, L1
Johns-Krull, C. M. 2007, ApJ, 664, 975
Johnson, D. R. H., & Soderblom, D. R. 1987, AJ, 93, 864
Karmakar, S., Pandey, J. C., Savanov, I. S., et al. 2016, MNRAS, 459, 3112
Kastner, J. H., Huenemoerder, D. P., Schulz, N. S., Canizares, C. R., & Weintraub, D. A. 2002, ApJ, 567, 434
Koenigl, A. 1991, ApJ, 370, L39
Lindegren, L., Lammers, U., Bastian, U., et al. 2016, A&A, 595, A4
Lindegren, L., Hernandez, J., Bombrun, A., et al. 2018, arXiv:1804.09366
Manara, C. F., Fedele, D., Herczeg, G. J., & Teixeira, P. S. 2016, A&A, 585, A136
Pandey, J. C., Singh, K. P., Drake, S. A., & Sagar, R. 2005, AJ, 130, 1231
Pojmanski, G. 2002, Acta Astronomica, 52, 397
Reipurth, B., & Zinnecker, H. 1993, A&A, 278, 81
Rigon, L., Scholz, A., Anderson, D., & West, R. 2017, MNRAS, 465, 3889
Roberts, D. H., Lehar, J., & Dreher, J. W. 1987, AJ, 93, 968
Robitaille, T. P., Whitney, B. A., Indebetouw, R., & Wood, K. 2007, ApJS, 169, 328
Robitaille, T. P., Whitney, B. A., Indebetouw, R., Wood, K., & Denzmore, P. 2006, ApJS, 167, 256
Robrade, J., & Schmitt, J. H. M. M. 2007, A&A, 473, 229
Rydgren, A. E. 1980, AJ, 85, 444
Scargle, J. D. 1981, ApJS, 45, 1
Shu, F., Najita, J., Ostriker, E., et al. 1994, ApJ, 429, 781
Siess, L., Dufour, E., & Forestini, M. 2000, A&A, 358, 593
Simon, T., Herbig, G., & Boesgaard, A. M. 1985, ApJ, 293, 551
Smith, R. K., Brickhouse, N. S., Liedahl, D. A., & Raymond, J. C. 2001, ApJ, 556, L91
Stassun, K. G., van den Berg, M., Feigelson, E., & Flaccomio, E. 2006, ApJ, 649, 914
Stelzer, B., & Schmitt, J. H. M. M. 2004, A&A, 418, 687
Strüder, L., Briel, U., Dennerl, K., et al. 2001, A&A, 365, L18
Turner, M. J. L., Abbey, A., Arnaud, M., et al. 2001, A&A, 365, L27
Vuong, M. H., Montmerle, T., Grosso, N., et al. 2003, A&A, 408, 581
Whitney, B. A., Indebetouw, R., Bjorkman, J. E., & Wood, K. 2004, ApJ, 617, 1177
Whitney, B. A., Wood, K., Bjorkman, J. E., & Cohen, M. 2003a, ApJ, 598, 1079
Whitney, B. A., Wood, K., Bjorkman, J. E., & Wolff, M. J. 2003b, ApJ, 591, 1049
Wright, E. L., Eisenhardt, P. R. M., Mainzer, A. K., et al. 2010, AJ, 140, 1868